EVALUATION OF CONJUGATE, RADIAL HEAT TRANSFER IN AN INTERNALLY INSULATED COMPOSITE PIPE

Niels Reurings[1], Sotiris Koussios[2], Otto K. Bergsma[3] and Karel Vergote[4]

[1]Aerospace Engineering, Delft University of Technology
Kluyverweg 1, Delft, The Netherlands
c.reurings@tudelft.nl, http://www.lr.tudelft.nl

[2]Aerospace Engineering, Delft University of Technology
Kluyverweg 1, Delft, The Netherlands
s.koussios@tudelft.nl, http://staff.tudelft.nl/S.Koussios/

[3]Aerospace Engineering, Delft University of Technology
Kluyverweg 1, Delft, The Netherlands
o.k.bergsma@tudelft.nl, http://staff.tudelft.nl/O.K.Bergsma/

[4]Bosal Emission Control Systems n.v.
Dellestraat 20, Lummen, Belgium
http://www.bosal.com

Keywords: Composite, Heat transfer, Thermal insulation, Experimental, Turbulent gas flow

ABSTRACT

In order to compete with steel, a fibre-reinforced composite exhaust wall with a general-purpose resin system requires an effective but lightweight insulation layer. However a lack of experimental methods for heat transfer from turbulent gas flow to pipe walls lined with a porous insulation layer was discovered in literature. Such a test method is crucial to assess the influence of the permeability of such an insulation layer on the heat transfer rate, such that the lightest configuration can be selected.

A new test method was developed and tested on samples representative for a composite exhaust. The accuracy of the method was assessed and the results for samples with different wall roughness were obtained. The behaviour of the samples under consideration proved to be more complicated than predicted by theories for impermeable pipe walls.

1 INTRODUCTION

Emission reduction stimulation by the European government has led to a higher priority for weight reduction amongst passenger car manufacturers [1]. As a result, the trend of the vehicle mass linearly increasing with the introduction of every new generation has been broken (see Figure 1). This was, in part, achieved by replacement of steel in cold structural components with fibre reinforced plastics.

However, for exhaust systems and other components exposed to temperatures above 600°C, the most obvious alternatives, high-end polymers and aluminium, are not applicable. In fact, there are very few cost-effective and lightweight alternatives to steel at such elevated temperatures. Lower density metals are generally more expensive than steel, the same holds for ceramics which are brittle furthermore.

Departing from single materials, a system solution is offered as an alternative. Combine fibre-reinforced plastic with an insulation layer to offer similar mechanical performance to steel at lower weight. For this to be feasible, the insulation has to be cost-effective and have good specific thermal performance. A schematic representation of the concept can be found in Figure 2.

Previous work has shown that insulation of the fibrous type is the most promising. The many types of currently available fibrous insulation are often used as thermal barrier in applications involving air, such as industrial ovens and catalytic convertor substrates. The project of the authors, however, focuses on a more demanding application of the insulated composite concept, namely passenger car

exhaust systems.

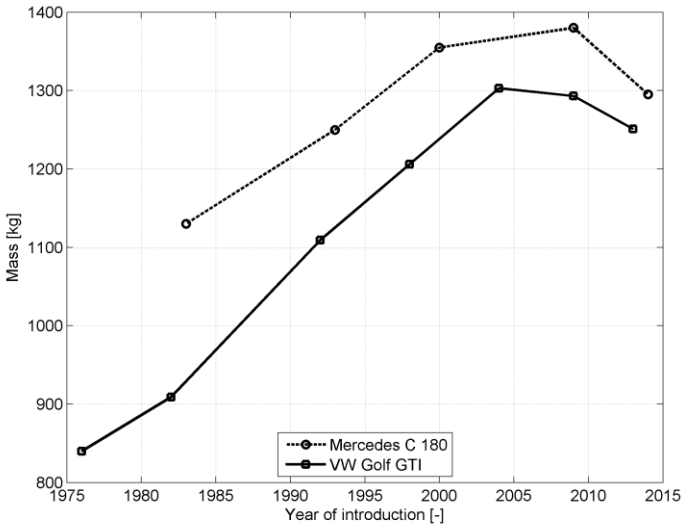

Figure 1 Vehicle mass versus year of introduction of two mid-sized passenger car models on the European market.

The literature regarding the static use of fibrous insulation has been well established, including several test standards such as ASTM C201 and C177 [2, 3]. However, in order to dimension the insulation for the current application requires assessment of the effect of turbulent flow on the heat transfer.

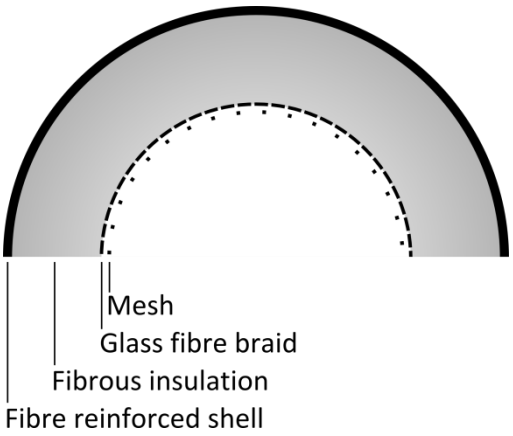

Figure 2: Schematic representation of half the cross-section of the composite exhaust concept.

The flow in an exhaust system can over the whole engine operating range be described as transient (pulsating) and due to high velocity (30-170 m/s) and high temperature (650-950 °C) also highly turbulent ($Re>1\cdot10^4$). The former is disregarded for now, but the interest with respect to flow conditions is in the turbulent, high temperature domain. Furthermore, the ideal thermal conductivity of the insulation would be lower than that of the gas.

Judging from the significant number of publications over the years, there is a large interest in the flow profile of and heat transfer from gas flow over and through fibrous insulation, or more general, porous media. Yet, due to the complexity of the problem only a few authors have published experimental results [4-9], but such publications are essential to validating any analytical or numerical model.

In 1967 Beavers and Joseph published their work on the flow profile in the laminar regime, but they did not consider heat transfer [4]. Zippe and Graf also considered a channel with walls lined with

a porous medium, but focussed on turbulent flow [5].

Angirasa on the other hand, focussed on the heat transfer from a small aluminium fibrous wall-mounted block to the turbulent air flowing over and past it. Because it covered only part of the wall, it had five of its sides exposed to the flow, making it hard to compare to completely lined walls. The heat transfer was determined through measurement of the temperature rise of the gas using thermocouples [6].

Using water instead of air as the moving medium, Prinos et al. were able to scale up the whole experiment for the same Reynolds number. This allowed them to measure the velocity distribution relatively close to the interface between the porous and open domain [7].

Pavel and Mohamad, and Huang et al. investigated the influence of the addition of a porous core to a pipe on the heat transfer from the moving medium to the outer wall [8, 9]. This affects the heat transfer at the wall in a different way compared to porous material lining the wall and is therefore less relevant to the modelling of an insulated wall.

In short, no experimental results were found on the heat transfer from turbulent flow to channel or pipe walls lined with a porous medium. The authors are of the opinion that, due to the lack of a validation possibility, the trends from analytical and numerical models concerning this case should be regarded with certain scepticism.

Furthermore, those three experimental investigations of the heat transfer used a porous medium with a thermal conductivity at least two order of magnitude larger than that of the fluid [6, 8, 9]. Conductivity will then have a much larger influence on the total heat transfer compared to an insulated wall.

This paper discusses the development of a test method for the heat transfer from turbulent gas to an insulated wall, such that regular composite shells can be applied at higher temperatures. Not only to assess steady flow as investigated in this work, but also to be able to investigate the effect of pulsation on the heat transfer in the future. This test method could, with some minor changes, also be used for more general porous media.

Not only the conductivity of the here applied porous materials is different compared to previously used metallic foams, also the permeability is different. One of the mechanisms behind fibrous insulation materials is a low permeability through which there is very little convection. The temperature and optical thickness of the porous medium will determined the extent to which radiation plays a part [10].

Beavers and Joseph, and Chan et al. have shown experimentally for laminar and numerically for turbulent bulk flow respectively, that at low values of permeability there is hardly any flow in the porous domain compared to the bulk velocity [4, 11].

As such, the authors will compare conventional pipe heat transfer equations for smooth and rough impermeable walls to the measured heat transfer to see to which extent these hold. Petukov presented the following two equations for the Nusselt number and friction factor f for a smooth wall respectively

$$Nu = \frac{(f/2)RePr}{1.07 + 12.7(f/2)^{1/2}(Pr^{2/3} - 1)} \quad (1)$$

$$f = \frac{1}{4\left(1.82\log_{10} Re - 1.64\right)^2} \quad (2)$$

where Re is the Reynolds number of the flow, which is a measure of the turbulence level of the flow and Pr is the Prandtl number of the fluid which expresses the relative effectiveness of thermal diffusion and convection [12]. Both equations are empirical, but applicable for $4{\cdot}10^3 \leq Re \leq 5{\cdot}10^5$ and $0.6 \leq Pr \leq 60$.

For rough walls, the heat transfer is an empirical function of the relative size of the roughness, the actual shape of the roughness elements, the channel cross-sectional shape [13]

$$Nu = St_w \cdot Re \cdot Pr \quad (3)$$

$$St_w = \frac{1}{\sqrt{2/f}\left(2.39\ln\left(\frac{D_e}{e}\right) + A_h - G'\right)} \quad (4)$$

where e is the actual roughness height, D_e is the equivalent diameter of the channel, A_h is a roughness parameter for heat transfer and G' is a geometry parameter. The

The Nusselt number is the most used figure to characterize heat transfer from a moving medium to a wall. It represents the ratio of convection heat transfer to fluid conduction heat transfer under the same conditions. In other words, the larger the Nusselt number, the more the situation differs from pure conductivity. For a pipe it is defined as

$$Nu = \frac{\alpha D}{k_f} \quad (5)$$

where α is the convective heat transfer coefficient (W/m^2·K), D is the diameter and k_f is the fluid thermal conductivity (W/m·K). Knowledge of the Nusselt number for a given insulated wall, would allow design of the insulation for the given composite shell.

2 METHOD

ASTM C177 and C201 are suitable to determine the heat transfer and effective conductivity of fibrous media under stationary conditions. The former measures the temperature difference over the insulation for a given heat input, while the latter controls the heat input required to maintain a certain temperature difference [2, 3]. The experiment described here, measures both the heat input and the temperature difference for maintained flow conditions.

More explicitly, the temperature difference over the insulation as well as the stream-wise drop in temperature of the heated gas over the test section is measured. The latter is used to determine the heat flux q (W/m^2), which is obtained according to;

$$q = \frac{c_p \dot{m}\, \Delta T_{gas}}{2\pi r_i l} \quad (6)$$

where c_p is the isobaric specific heat capacity of the gas, $\dot{m}$ is the mass flow in kg/s, ΔT_{gas} is the temperature drop of the bulk gas stream over the sample length in Kelvin, r_i (m) is the inner radius of the sample and l (m) is the distance between the two thermocouples measuring the gas temperature at both ends of the sample.

Due to the use of a gas burner, the composition of the flowing medium is no longer that of normal air. As a result, the fluid properties for the flue gas have to be used. The estimation of the flue gas properties was done according to the parametric equations and coefficients provided in ref. [14]. The mole fractions were estimated based on the expected combustion products of natural gas with a hydrogen content of 19% at complete combustion.

2.1 Setup

In Figure 3 a schematic representation of the test setup is shown. From up to downstream, the gas flow gets heated in the burner, moves through the contraction section to a regular pipe section and then enters the front connector of the sample (see also Figure 4). Downstream of the sample is another identical connector which guides the flow through another cylindrical section, towards the heat exchanger and flow meter respectively, before it exits the setup outside the test cell through an open end.

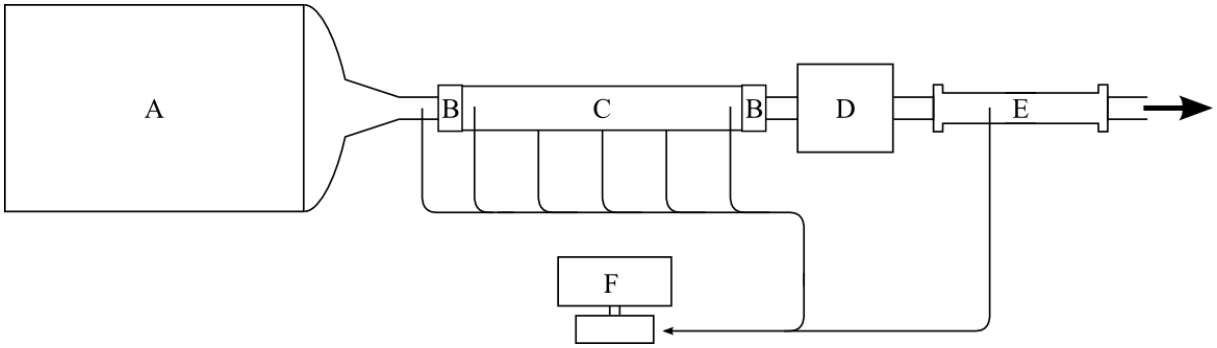

Figure 3: Schematic representation of the test setup. The lines are drawn from thermocouple locations to the data logging system. The following components are labeled; A=burner, B=steel-composite connector, C=internally insulation composite pipe test section, D=heat exchanger, E=flow meter, F=data logging system.

The custom built IBS natural gas burner (component A in Figure 3) provides the test section with hot flue gas at the desired temperature and mass flow rate. It can provide 750 Nm^3/h of flue gas at temperatures up to 1100 °C. Downstream of the burner and the conical flow director, but ahead of the sample is a metal sheathed K-type thermocouple which serves as a reference for the inlet gas temperature. Furthermore, it provides an indication of the heat lost over the upstream connector (left B in Figure 3).

The flow meter (component E, ABB torbar) is more accurate than the mass flow given by the burner, but its calibration tolerances (±1%) are valid only below 400 °C hence the upstream addition of the heat exchanger (D). The data is logged every 5 seconds using IMC Spartan soft- and hardware, which is calibrated at ±1 °C from thermocouple connection to software data logging.

Given the unknown influence of the porous domain on the velocity and temperature profile, it is assumed that both profiles still have to develop, which, given the turbulent nature of the flow, means that about 6 diameters downstream of the entrance, there is a fully developed thermal situation [15, 16].

The change of temperature of the gas over the composite section is measured using Inconel 600 sheathed K-type thermocouples of 1.5 mm in diameter with a tolerance of ±0.4% supplied by Thermo Electric (Waddinxveen, The Netherlands). These thermocouples protrude transversely into the core of the flow. Since the flow is highly turbulent, a flat temperature distribution can be assumed and hence, the measured core temperature is assumed to be the bulk temperature of the gas flow.

The other thermocouples are also K-type but not sheathed and are of a different tolerance class (the larger of 2.2 °C and 0.75%). The wire insulation of the thermocouples applied on the shell is PTFE and that of those inside the insulation is E-glass.

2.2 Samples

Heuer et al. have shown that the fibre loss rate of unprotected high porosity, binderless, fibrous insulation is significant and this would disqualify the samples for repeatability and long-term testing [17]. As such, a braid was added to cover the insulation. The braid is thin and permeable to a certain extent, but it limits interaction of the open flow with the air inside the porous domain.

The samples are designed according to the concept shown in Figure 2, so a composite outer shell lined with a fibrous insulation layer, which is protected and kept in place by an E-glass braid and a wire mesh. These were manufactured around a 50 mm diameter reference pipe; the inner diameters are therefore slightly larger (51 and 53 mm respectively).

	Sample I	Sample III
Resin	Hexion EPIKOTE 04908	Two component epoxy resin system
Glass fibre	HexForce 07581, 8 harness satin weave, E-glass (Hexcel, United States)	
Insulation	Fibrous insulation 160 kg/m^3	Fibrous insulation 190 kg/m^3

	(Morgan Thermal Ceramics, UK)	(Morgan Thermal Ceramics, UK)
Braid	E-glass braid, φ=55mm, t=~0.3mm	
Mesh	Stainless steel, t_{wire}=0.07mm, 25% open, Haver & Boecker, Germany	Zinc coated steel, t_{wire}=0.55mm, 91% open, (Karwei, The Netherlands)
Adhesive	Two component epoxy adhesive	

Table 1: Sample properties

Both insulation materials have the same fibre composition and diameter (<10 µm). Even the base density of both types is the same (128 kg/m3), but this has been increased to different values due to compression inside the sample. The manufacturer specified effective conductivity established using ASTM C201 is in the order of 0.10 W/mK. Both insulation types are of the blanket type, i.e. no binder or hardener, and are certified at sufficiently high temperatures for exhaust application. Based on the bulk density and the specified composition of the insulation, the porosity was estimated at more than 90% for all samples.

The braid and insulation have negligible stiffness and to prevent collapse due to the Venturi effect and to compress the insulation to the specified density, the wire mesh has been added. On the outside, the thermoset glass fibre-reinforced shells of samples I and III have glass transition temperatures of 90 and 200 °C respectively, a quasi-isotropic lay-up and a thickness of roughly 1mm.

The insulation material and its density, the resin system and the wire mesh varied between the samples, for all specifications see Table 1.

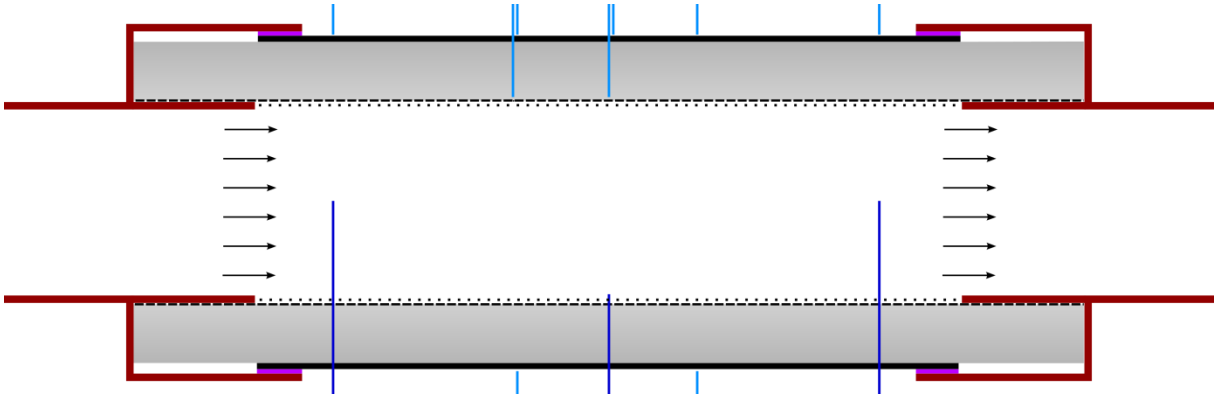

Figure 4: A schematic representation of the test samples used. The connectors are shown in red, the insulation in gray, the adhesive in purple and the fibre-reinforced shell in black. The dark blue lines are the sheathed K-type thermocouples, whereas the light blue ones are unsheathed.

In Figure 4 all thermocouple locations are indicated. The two sheathed ones protruding into the gas stream were at a distance of 0.05 m from the connector edges and 0.75 m apart. An additional one was positioned just through the braid and mesh and into the gas flow, halfway down the sample.

Furthermore, seven thermocouples were placed symmetrically on the outside of the sample, five at the top and two at the bottom of the cross-section. Those five were at 0.05, 0.30, 0.425, 0.55 and 0.80 m from the upstream connector edge and the two at the bottom were are at 0.30 and 0.55 m from the upstream connector edge.

Two glass fibre shielded thermocouples were placed such that their tip would be at the inner end of the insulation, touching the glass braid. These were placed at an angle, such that the insulation radially outward was not influenced.

The connectors are made of 1 mm thick AISI 304 steel and were filled with the same insulation material as the sample. The conductive path length between cylinder and composite (1.5 cm radially and 20 cm longitudinally) was sufficiently long to have the steel drop to temperatures not exceeding 300 °C (see Figure 4).

In order to have an airtight sample section, a physical connection between the composite shell and the rest of the setup is necessary. The connectors were therefore adhered to the composite shell with an

overlap length of 2 cm. The adhesive retains a useful portion of its strength at temperatures exceeding 200 °C and has a specified thermal conductivity of 0.4 W/mK.

The composite shell is therefore not fully decoupled from the rest of the system, but the amount of heat transferred from the connectors to it is less than 10% of the heat coming through the insulation. The thermal conductivity of the glass fibre composite is in the order of unity and to exclude any influence of the connectors, only the readings of the five middle thermocouples were used for the outer shell temperature [18].

The inaccuracy of the gas temperature measurement was ±1.0 °C and ±0.4 %, which means that for a single thermocouple measurement the inaccuracy ranges between ±2.4 °C and ±3.5 °C at gas temperatures of 350 and 635 °C respectively. The temperature drop is obtained from the difference between two sensors and its uncertainty is therefore double these values, so between 4.8 and 7.0 °C.

2.3 The test procedure

For a given mass flow, the temperature was increased in steps of roughly 50 °C, covering a temperature range between 350 and 500 °C for sample I, which has the lower resin glass transition temperature. This was done at the mass flows of 240, 290 and 350 kg/h. The corresponding range of Reynolds number is $4.4 \cdot 10^4$-$7.8 \cdot 10^4$.

The second sample was able to withstand higher inlet temperatures, as such the temperature range was increased to 350-650 °C and the mass flows tested were 240, 290, 350 and 400 kg/h. This corresponds to Reynolds numbers between $3.6 \cdot 10^4$ and $8.6 \cdot 10^4$.

Upon a change of burner specified temperature, it takes about 20 second for the gas to reach the new temperature. Due to the presence of the insulation with its corresponding thermal mass and low conductivity, it takes about 650 seconds after that for the shell to reach the new equilibrium temperature. The gas temperature change can therefore be considered a step change with respect to the shell and exponential convergence towards equilibrium is expected. In Figure 5 an exponential line is fit through the measured temperature at the middle of the sample after the gas has reached its new equilibrium temperature, the two lines match well.

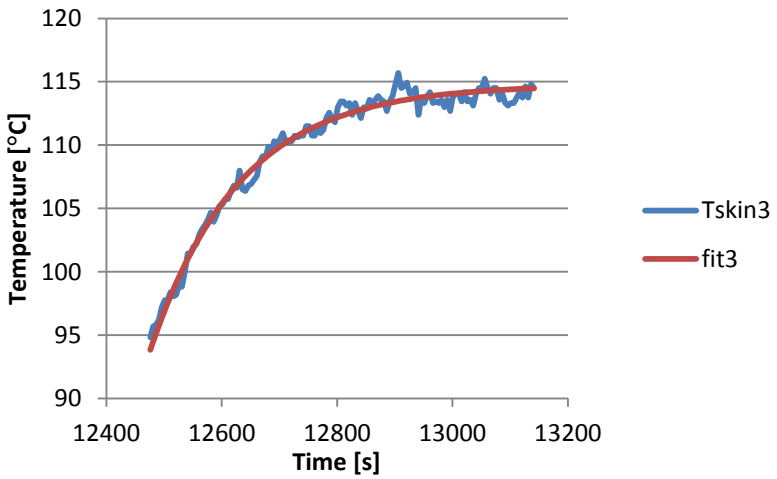

Figure 5 Temperature change of the shell of sample III after inlet gas temperature step change from 430 to 525 °C at 400 kg/h (blue) together with exponential fit (red).

3 RESULTS AND DISCUSSION

The measured drop in temperature of the gas over the test section is shown in Figure 6. The relative drop in temperature with respect to the inlet gas temperature ranges between 2.1 and 4.3%. The larger the inlet gas temperature, the larger the temperature difference with ambient and thus the larger the heat transfer through the wall and the corresponding temperature drop.

Apart from this, it can be found from Figure 6 that the temperature drop decreases with increasing mass flow. The larger the mass flow, the larger the total thermal mass that flows through the sample per unit of time. If the heat transfer through the wall does not change accordingly, then the total

temperature drop will be smaller. And indeed, the mass flow dependency of the power is weak, which is reflected also in the small almost overlapping lines in Figure 7 for different mass flow rates.

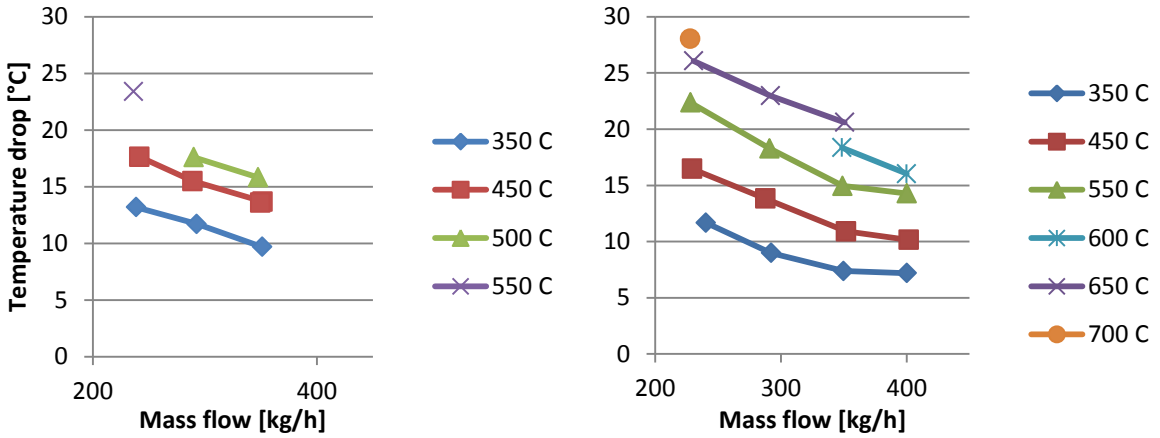

Figure 6 Measured temperature drop of the flue gas over the test section as a function of mass flow rate and mean gas temperature of sample I (left) and sample III (right).

The inaccuracy in the gas temperature difference discussed earlier makes up a significant portion of the measured difference, especially for the measurements at 350 and 450 °C. Until the accuracy can be improved, all conclusions regarding absolute values should therefore be treated with care.

On the other hand, the exact same thermocouples were used at the same locations for both samples and the systematic errors are therefore assumed to be similar for all measurement points. Furthermore, since the equilibrium situation is of interest, a long measurement time is possible. By averaging over this time, one can limit the influence of scatter. In Figure 7, the error bars indicate the 95% variation with time interval.

Given the magnitude of the scatter, relative comparisons with respect to the different conditions can therefore be made. Future setup improvement might result in sufficient measurement accuracy for absolute performance quantification of insulation materials.

From the measured drop in temperature and using the numerator of Equation (6), one obtains the total heat lost by the gas over the test section (see Figure 7) for the tested mass flow and temperature combinations. As mentioned before, this amount of power is just a few percent of the thermal energy of the exhaust gasses.

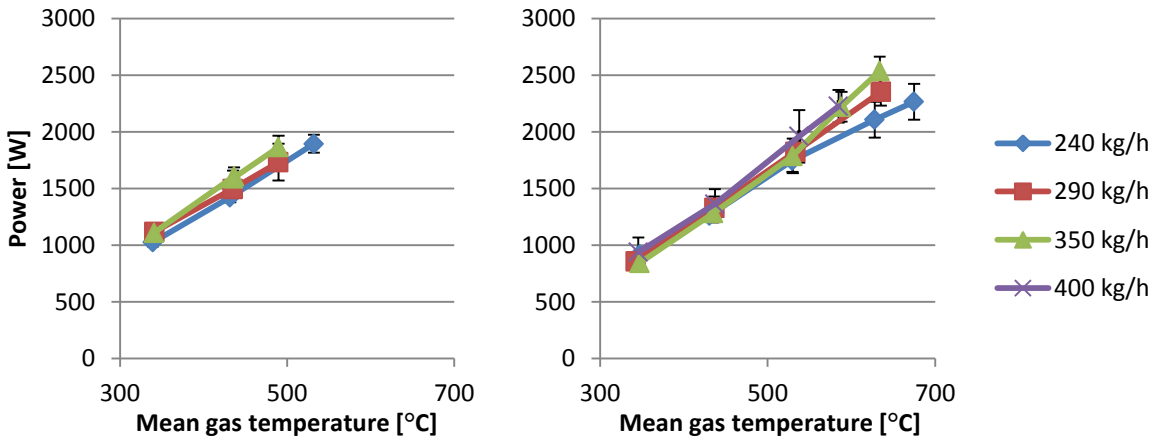

Figure 7 Measured power loss of the flue gas over the test section of sample I (left) and sample III (right) as a function of mean gas temperature and mass flow rate. The error bars indicate the 95% range of time variation at equilibrium.

In order to compute the Nusselt number for the two tested samples, one requires the convective heat transfer coefficient α, which can is obtained by dividing q by the temperature difference between

the gas and the temperature measured just below the braid. The resulting Nusselt numbers are shown in Figure 8 and Figure 9. Also shown are the theoretical lines for hydraulically smooth and rough, impermeable walls from equations (1) and (3) respectively.

The magnitude of both theoretical Nusselt numbers is comparable. Furthermore both predict a Reynolds dependence that is stronger than measured. In a smooth pipe a higher Reynolds number leads to a thinner boundary layer and therefore a larger temperature gradient, hence a larger Nusselt number.

Sample I however lacks a truly smooth wall; according to the Moody diagram it is between hydraulically smooth and rough depending on the flow condition [19]. Hence at a certain point its boundary cannot become any thinner and the turbulence dependence changes. This could explain why, for the lower mass flow rates, the trend is upward, while for the highest rate it is more or less flat.

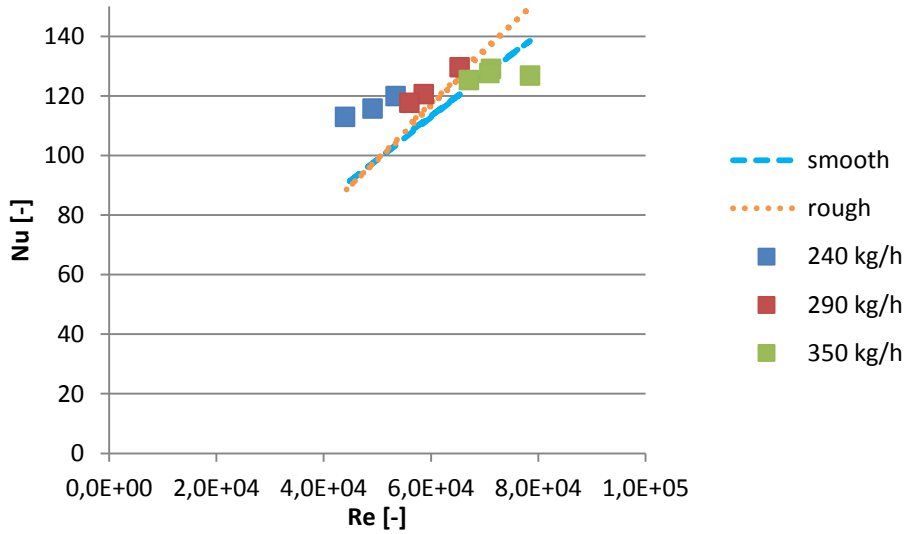

Figure 8 Nusselt number from theory (dashes) and from measurement (solid squares) for sample I as a function of the Reynolds number and the mass flow rate.

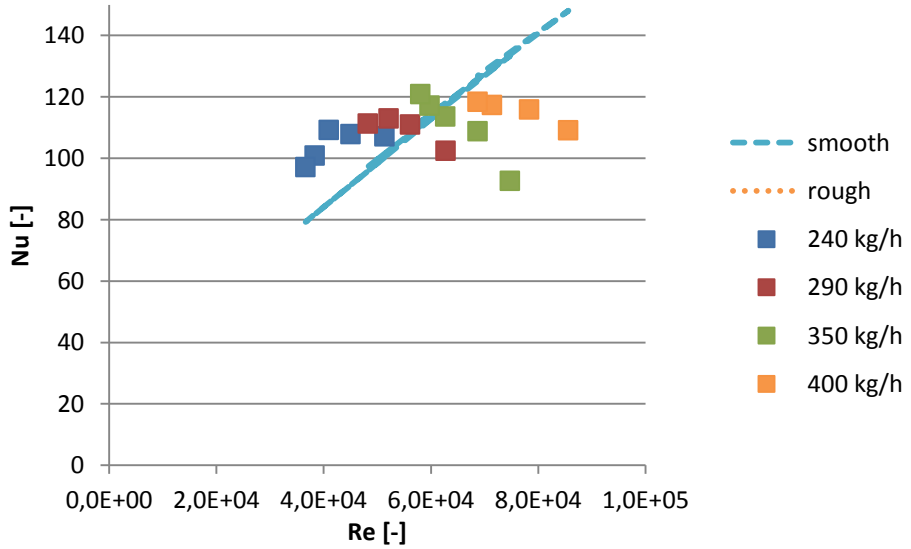

Figure 9 Nusselt number from theory (dashes) and from measurement (solid squares) for sample III as function of the Reynolds number and the mass flow rate. The rough line is off the chart.

In Figure 9 the behavior of sample III as a function of the Reynolds number is more complex. For all four mass flows, there might be a maximum close to the theoretical line for a smooth wall. The difference with the theory for a smooth line is significant, as expected given the wall roughness.

Comparing the data points for 290 and 350 kg/h between the two samples shows a change in trend, from increasing with turbulence to decreasing.

To get more insight, also look at the temperature dependence in Figure 10. It does not show the strong mass flow dependence of the theory for smooth wall, nor the downward trend with increasing temperature. But neither does the theory for rough walled pipes, which was also plotted in Figure 9 and Figure 10 but was cropped for the readability. The theory for rough walls predicts values in the range of 250-430, which is more than three times the measured values.

Yet if the differences were due to permeability, then one would expect an increase in Nusselt number with increasing Reynolds number and mass flow, due to increased interaction between the bulk air flow and the air in the porous domain.

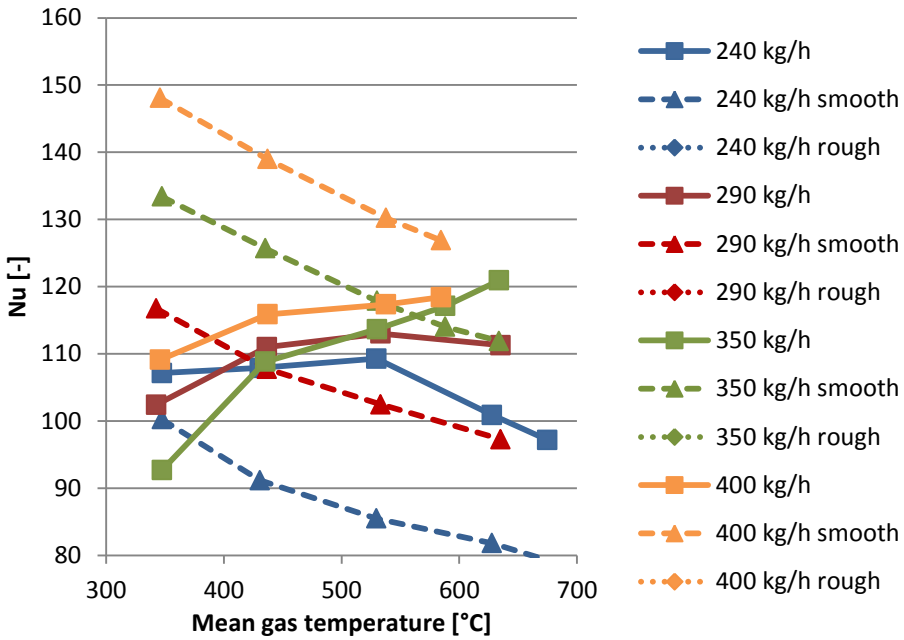

Figure 10: Nusselt number as a function of the mean gas flow rate for sample III for different mean gas temperatures according to theory (dashed lines) and measurement (solid lines). The rough lines are off the chart.

4 CONCLUSIONS AND RECOMMENDATIONS

The temperature drop over the sample is small enough to assume a constant gas temperature. Since the difference in temperature over the sample is required for the heat flux determination it is critical to minimize the measurement inaccuracy. It is recommended to use multiple thermocouples at each location and possibly swap location to assess the effect.

Sufficient improvement in accuracy would make this method well suited to measure the effective conductivity of the insulation material used, so far only the heat transfer from the gas to the wall directly next to the gas has been analyzed.

The difference of the mesh type (wall roughness) is clear from the results, with the smooth sample showing Nusselt numbers close to those found from smooth wall theory. The sample with coarse mesh showed a similar magnitude in Nusselt number but different behavior with respect to flow parameters.

In the future truly impermeable samples will also be used to discern the effect of roughness and permeability. Furthermore other insulated samples will be tested to assess the effects of insulation density on the heat transfer.

ACKNOWLEDGEMENTS

The authors want to thank the technicians at both BOSAL ECS n.v. and the Delft Aerospace Structures and Materials Laboratory for their support, as well as prof.dr.ir. R. Benedictus for an

insightful discussion. The authors also want to thank the Belgian agency for Innovation by Science and Technology (IWT) for their financial support.

REFERENCES

[1] European Union, "Regulation (EU) 715-2007," *OJ L 171*, pp. 1-16, 29.06.2007 2007.
[2] ASTM, "C201 - Standard Test Method for Thermal Conductivity of Refractories," ed: ASTM International, 2013.
[3] ASTM, "C177 - Standard Test Method for Steady-State Heat Flux Measurements and Thermal Transmission Properties by Means of the Guarded-Hot-Plate Apparatus," ed: ASTM International, 2013.
[4] G. S. Beavers and D. D. Joseph, "Boundary conditions at a naturally permeable wall," *Journal of Fluid Mechanics,* vol. 30, pp. 197-&, 1967.
[5] H. J. Zippe and W. H. Graf, "Turbulent boundary-layer flow over permeable and non-permeable rough surfaces," *Journal of Hydraulic Research,* vol. 21, pp. 51-65, 1983.
[6] D. Angirasa, "Experimental investigation of forced convection heat transfer augmentation with metallic fibrous materials," *International Journal of Heat and Mass Transfer,* vol. 45, pp. 919-922, Feb 2002.
[7] P. Prinos, D. Sofialidis, and E. Keramaris, "Turbulent Flow Over and Within a Porous Bed," *Journal of Hydraulic Engineering,* vol. 129, pp. 720-733, Sep 2003.
[8] B. I. Pavel and A. A. Mohamad, "An experimental and numerical study on heat transfer enhancement for gas heat exchangers fitted with porous media," *International Journal of Heat and Mass Transfer,* vol. 47, pp. 4939-4952, Nov 2004.
[9] Z. F. Huang, A. Nakayama, K. Yang, C. Yang, and W. Liu, "Enhancing heat transfer in the core flow by using porous medium insert in a tube," *International Journal of Heat and Mass Transfer,* vol. 53, pp. 1164-1174, Feb 2010.
[10] H. Reiss, "K6 Superinsulations," in *VDI Heat Atlas*, VDI e. V., Ed., Second ed Heidelberg: Springer-Verlag, 2010.
[11] H. C. Chan, W. C. Huang, J. M. Leu, and C. J. Lai, "Macroscopic modeling of turbulent flow over a porous medium," *International Journal of Heat and Fluid Flow,* vol. 28, pp. 1157-1166, Oct 2007.
[12] B. S. Petukov, "Heat transfer and friction in turbulent pipe flow with variable physical properties," *Advances in Heat Transfer,* vol. 6, pp. 503-564, 1970.
[13] Engineering Sciences Data Unit (ESDU), "Pressure loss and heat transfer for single-phase turbulent flow in roughened channels: methods of calculation," IHS ESDU1983.
[14] M. Kleiber and R. Joh, "D1 Calculation Methods for Thermophysical Properties," in *VDI Heat Atlas*, VDI e. V., Ed., Second ed Heidelberg: Springer-Verlag, 2010.
[15] L. M. K. Boelter, G. Young, and H. W. Iverson, "An investigation of aircraft heaters XXVII - Distribution of heat-transfer rate in the entrance section of a circular tube," National Advisory Committee for Aeronautics - University of California, Washington1948.
[16] A. F. Mills, "Experimental investigation of turbulent heat transfer in the entrance region of a circular conduit," *Journal of Mechanical Engineering Sciences,* vol. 4, pp. 63-77, 1962.
[17] V. Heuer and G. Walter, "Wear of Fibrous Ceramic Components Caused by High Velocity Gas Streams: Erosion Mechanisms," *Ceramic Forum International / Ber. DKG,* vol. 75, pp. 29-35, Nov-Dec 1998.
[18] Granta Design Limited, "CES Edupack 2013 v12.2.13," ed, 2013.
[19] L. F. Moody, "Friction factors for pipe flow," *Trans. ASME,* vol. 66, 1944.